Editors' Suggestion

Timing Correlated-Electron Emission from Strong Field Atomic Double Ionization with Polarization-Gated Attoclock

YanLan Wang,* ShaoGang Yu,* RenPing Sun, HuiPeng Kang, SongPo Xu, XuanYang Lai, Wei Quan, and XiaoJun Liu†

State Key Laboratory of Magnetic Resonance and Atomic and Molecular Physics, Wuhan Institute of Physics and Mathematics, Innovation Academy for Precision Measurement Science and Technology, Chinese Academy of Sciences, Wuhan 430071, China

(Received 7 February 2024; accepted 1 May 2024; published 30 May 2024)

Attoclock provides a powerful tool for probing the ultrafast electron dynamics in strong laser fields. However, this technique has remained restricted to single electron or sequential double ionized electron dynamics. Here, we propose a novel attoclock scheme with a polarization-gated few-cycle laser pulse and demonstrate its application in timing the correlated-electron emission in strong field double ionization of argon. Our experimental measurements reveal that the correlated-electron emission occurs mainly through two channels with time differences of 234 ± 22 as and 1043 ± 73 as, respectively. Classical model calculations well reproduce the experimental results and deepen our understanding of ultrafast electron correlation dynamics.

DOI: 10.1103/PhysRevLett.132.223202

Tracing the motion of the electrons on its characteristic timescale provides an effective way to identify and understand the essential features of many ultrafast photophysics and photochemical processes. Among all the attosecond metrology techniques [1–8] capable of resolving electron dynamics on attosecond (as) timescales, the attosecond angular streaking (or attoclock) technique [7,8] holds particular significance due to its ability for self-referencing and feasibility with a femtosecond (fs) laser pulse. This technique utilizes a strong, nearly circularly polarized infrared laser pulse to ionize atoms or molecules. The rotating electric field vector deflects the photo-ionized electron into a certain direction depending on the moment it escapes from the atom. Specifically, the ionization moment within one laser cycle (e.g., ~2.7 fs for $\lambda \sim 800$ nm) will be mapped to the 360° interval of the final emission angles (where 1° corresponds to ~7.4 as) in the polarization plane. Thus, by analyzing the angle-resolved photoelectron spectrum, the ionization time of the photoelectrons can be determined with an accuracy as high as a few attoseconds. The attoclock technique has been widely applied to explore tunneling time [7–19], the resonant ionization time delay [20] of electron in single ionization process, and also emission time difference between two electrons in sequential double ionization process [21–27]. Despite the great success of attoclock technique in timing the individual electron dynamics, its application to correlated-electron dynamics in strong field, such as emission of the two electrons in nonsequential double ionization (NSDI) process [28] (for recent reviews, see, e.g., Refs. [29–31]), remains a challenge. A major obstacle is closely related to the fact that, under a circularly or elliptically polarized laser field employed in attoclock, the multielectron emission usually occurs in a sequential way and the electron correlation dynamics is strongly suppressed [32].

In this Letter, we report on a novel attoclock experiment aimed at circumventing this issue by employing a polarization-gated (PG) laser pulse. As shown in Fig. 1(a), the PG pulse consists of two counter-rotating circularly polarized, time-delayed, and carrier-envelope phase (CEP) stabilized few-cycle laser pulses. The combined pulse has a time-dependent ellipticity in overlapping temporal region [33–38], in which the central portion exhibits approximately linear polarization (labeled as gate) while the remaining regions exhibit elliptical polarization, as illustrated in Fig. 1(b). As a result, the PG pulse can effectively drive two electrons emission in a correlated way within the gate, while also possessing the property of angular streaking. Consequently, it can be used to trace the release times of the two correlated electrons. Here, we utilize the intrinsic property of PG attoclock to investigate the decaying process of the recollision-induced doubly excited complex (DEC) in the strong field nonsequential double ionization of argon atom.

A diagram of the PG attoclock experiment is depicted in Fig. 1(c). Choosing a low intensity of $I = 8.5 \times 10^{13}$ W/cm^2 and a center wavelength of $\lambda \sim 760$ nm for the combined PG pulse, a DEC Ar^{**} is induced by the recollision in the NSDI process of argon [39–41]. The DEC subsequently decays via $Ar^{**} \rightarrow Ar^{2+} + 2e^-$ into the double ionization continuum state with the assistance of the laser field within a very short time. The instants of the first (at t_1) and second (at t_2) ionization steps (the first and the second electrons are defined by their final ionization

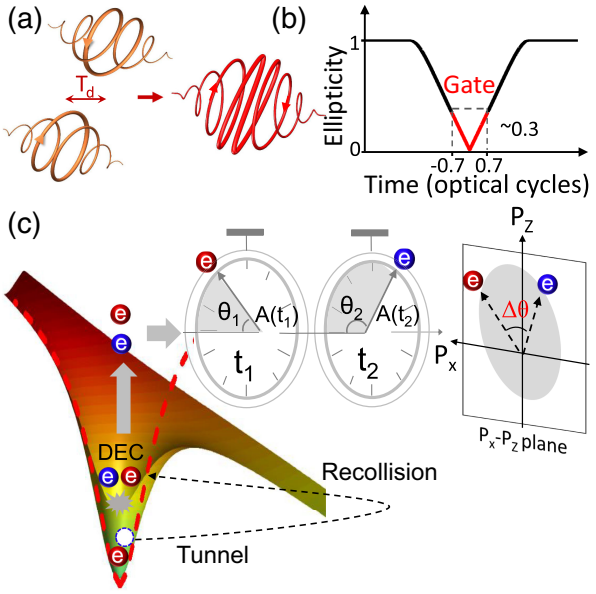

FIG. 1. (a) Schematic illustration of the construction of the PG pulse with two counter-rotating circularly polarized, time-delayed, and CEP stabilized few-cycle laser pulses. (b) The time-dependent ellipticity of the PG pulse used in the experiment. The central portion exhibits approximately linear polarization, which is referred to as a gate. (c) Process of excitation and field-assisted decay of the DEC. For each double ionization event, the ionization time $t_{1(2)}$ of the electron is defined as the instant when the electron is released into the continuum with zero kinetic energy. θ represents the angle of two emitted electrons relative to the x axis in the polarization plane. $\mathbf{A}(t_{1(2)})$ is the electric field vector potential at the ionization time of $t_{1(2)}$.

order) are mapped onto the emission angle of the electrons, i.e., θ_1 and θ_2, in the polarization plane of the PG pulse, which can be extracted from the measured electron angular distributions within the attoclock scheme. Our results show that the emission of the electron pairs is mainly through two channels, and the most likely emission time differences between the two electrons are revealed to be 234 ± 22 as and 1043 ± 73 as for these two channels, respectively. Classical trajectory Monte Carlo (CTMC) model calculations well reproduce the experimental measurements and allow us to comprehend the effect of the final-state electron-electron (e-e) repulsion in correlated-electron dynamics deeply.

In our experiment, a PG laser pulse is produced by propagating a linearly polarized, CEP stabilized few-cycle laser pulse with a center wavelength of 760 nm and a pulse duration as short as 5 fs through a birefringent quartz plate of specified thickness in conjunction with an achromatic $\lambda/4$ wavelength plate [38]. The CEP of the few-cycle pulse is calibrated by the asymmetry of the measured Ar^+ momentum distribution [42]. The intensity of the few-cycle pulse is calibrated with a procedure utilizing the photoelectron momentum distribution in a nearly circularly polarized laser field [43]. The time delay T_d between these two circularly polarized pulses is controlled by changing the thickness of the birefringent quartz plate and it is calibrated to be $T_d = 2.08T$ (T is optical period) by using the photoelectron momentum distribution measured in coincidence with Ar^+ in single ionization experiment [38]. By focusing the CEP-stabilized PG laser pulses through an on-axis spherical mirror ($f = 75$ mm) onto a supersonic Ar beam in an ultrahigh vacuum chamber of a cold target recoil ion momentum spectrometer [44–46], one of the two photoelectrons and the Ar^{2+} ion ejected from double ionization of Ar are detected in coincidence, and we obtain the momentum of the undetected electron by exploiting the momentum conservation between the two electrons and the Ar^{2+} ion.

The measured correlated-electron angular distributions (CEADs) of double ionization of Ar are shown in Figs. 2(a) and 2(b) for CEP $\varphi = 0.7\pi$ and 1.2π, respectively. The spectra are symmetric with respect to $\theta_{e1} = \theta_{e2}$ diagonal because the two electrons are not distinguished in the experiment. One can see that both electrons prefer to emit in the direction of 90° or 270°, and main spectral peaks (labeled with Channel I) locate at about (270°, 270°) and (90°, 90°) for CEP $\varphi = 0.7\pi$ and 1.2π, respectively. A closer inspection shows that the majority of the distribution is not located on the diagonal, indicating that there exists a small angle difference between the two electrons from NSDI of Ar in the PG pulse. Besides the main peaks in the spectra, there are two weaker peaks (labeled with Channel II) around both (90°, 270°) and (270°, 90°), which correspond to the distribution of antiparallel emitted electron pairs.

To get an insight into the two electron emission dynamic of Ar in the PG pulse, we perform a 3D CTMC model calculation that fully considers the influence of the ionic Coulomb potential for the two electrons and the Coulomb repulsion between the two electrons (CTMC-CP) [47,48] (details of calculation are described in the Appendix). In the calculations, the electric field components of the PG pulse in the polarization plane (i.e., in z and x directions) used here are $E_z(t) = E_0\{\cos^2[\omega(t - T_d/2)/2n] + \cos^2[\omega(t + T_d/2)/2n]\}\cos(\omega t + \varphi)$ and $E_x(t) = E_0\{-\cos^2[\omega(t - T_d/2)/2n] + \cos^2[\omega(t + T_d/2)/2n]\} \times \sin(\omega t + \varphi)$, where E_0 is the maximum electric field amplitude, ω is the frequency, $n = 7$ is the number of optical cycles, and φ is the CEP for each circularly polarized pulse. T_d is the time delay between the two pulses. The CTMC model simulated results are shown in Figs. 2(c) and 2(d), which exhibit a rather good agreement with the experimental data, although a wider angular distribution is discernible for the latter [49].

In light of the good agreement between the simulation and experiment, a more comprehensive understanding of electron dynamics can now be achieved by analyzing the time distribution of the laser-driven electron trajectories. Figures 2(e) and 2(f) show the calculated time distribution

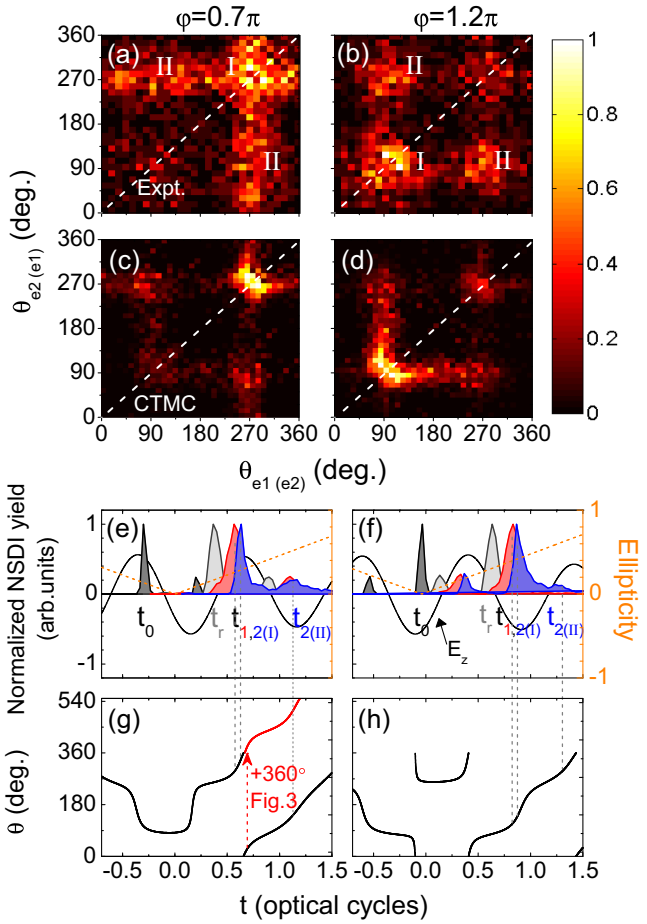

FIG. 2. The measured (a),(b) and CTMC-simulated (c),(d) correlated-electron angular distribution for $\varphi = 0.7\pi$ and $\varphi = 1.2\pi$, respectively. (e),(f) The CTMC calculated time distribution of the tunnel t_0 (black), recollision t_r (gray), ionization of the first t_1 (red), and second t_2 (blue) electrons in NSDI of Ar. The electric field component in the major polarization z axis (black line) and the ellipticity of the PG pulse (orange dashed line) are also shown in (e) and (f). (g),(h) The angular mappings of the electrons as a function of their emission time via the relation of $\mathbf{p} = -\mathbf{A}(t)$. The electron emission angle from the next laser cycle for $\varphi = 0.7\pi$ has been added by an additional 360° [red line in (g)]; see text for details.

of the tunnel t_0 (black), recollision t_r (gray), ionization of the first t_1 (red) and second t_2 (blue) electron trajectories in NSDI of Ar, together with the temporal profile of the laser electric field component along z axis for these two CEPs. The exponential growth of ionization rates with electric field strength [50] ensures that electrons mainly tunnel at the time of the electric field maximum (i.e., t_0). These tunneled electrons return around $t_0 + 0.75T$ (i.e., t_r), which is zero crossing point of the electric field [51], leading to the formation of the DEC. Subsequently, one electron will be ionized from the DEC nearby the next peak of the electric field (i.e., t_1). And most of the second electrons will be ionized soon after the first electrons (i.e., $t_{2(\mathrm{I})}$). However, if the second electron does not obtain enough energy from the laser field within this peak, it may be ionized nearby the next peak of the electric field (i.e., $t_{2(\mathrm{II})}$). The time-angle relations obtained from the vector potential of the PG electric field based on $\mathbf{p} = -\mathbf{A}(t)$ [52,53] for $\varphi = 0.7\pi$ and $\varphi = 1.2\pi$ are shown in Figs. 2(g) and 2(h), respectively. Here, the emission time windows of the two electrons are mainly confined within single cycle, thereby establishing a straightforward and unambiguous time-angle relation for the electron emission. Consequently, the two electrons can be distinguished by their emission angles. By mapping the ionization time distributions of t_1 and t_2 to the angular distributions, a comprehensive understanding of the CEADs is achieved. For $\varphi = 0.7\pi$, as an example, one can see that the main peak nearby (270°, 270°) in Channel I in the CEADs mainly comes from the electron pairs emitted at t_1 and $t_{2(\mathrm{I})}$, while the two small peaks in Channel II mainly come from the electron pairs emitted at t_1 and $t_{2(\mathrm{II})}$.

To retrieve the most likely emission time of the two electrons from the measured photoelectron angular distribution, we extract emission angular distributions of the distinguished first and second ionized electrons at $\varphi = 0.7\pi$ and $\varphi = 1.2\pi$ for different channels in Figs. 3(a1)–3(d2). For the convenience of analysis but without losing the physics, we add 360° to the emission angle from the next laser cycle [see the red curve in Fig. 2(g)] in the case of $\varphi = 0.7\pi$ to make the angle of the second ionized electron be larger than the first ionized electron. The angular distribution of the first and second ionized electrons is fitted with a Gaussian function to extract the location of the peak. For Channel I, the peaks locate at $\theta_1 = 259°$ and $\theta_2 = 284°$ for $\varphi = 0.7\pi$, while at $\theta_1 = 82°$ and $\theta_2 = 119°$ for $\varphi = 1.2\pi$, respectively. For Channel II, the peaks are at $\theta_1 = 263°$ and $\theta_2 = 437°$ for $\varphi = 0.7\pi$, while at $\theta_1 = 86°$ and $\theta_2 = 256°$ for $\varphi = 1.2\pi$, respectively. The peaks for the angular distribution of the first and second ionized electrons are also well reproduced by the CTMC calculations. Subsequently, in the context of attoclock scheme, by mapping the peaks of the angular distributions of the two electrons via the relation of $\mathbf{p} = -\mathbf{A}(t)$ [orange solid lines in Figs. 3(a3)–3(d3)] to their emission time, we extract the emission time differences of 456 ± 54 as for $\varphi = 0.7\pi$ and 431 ± 36 as for $\varphi = 1.2\pi$ in the case of Channel I and 1125 ± 88 as for $\varphi = 0.7\pi$ and 1092 ± 34 as for $\varphi = 1.2\pi$ in the case of Channel II, respectively.

It is worth noting that for correlated-electron emission, the influence of final-state e-e repulsion on the formation of angular distributions should be meticulously considered, particularly for Channel I where the emitted angular difference between the two electrons is very small. Therefore, we perform an additional CTMC calculation with Yukawa potential (CTMC-YP) to elucidate the influence of the final-state e-e Coulomb repulsion on the extracted emission time difference. In the calculation, the Coulomb potential between the two electrons is substituted

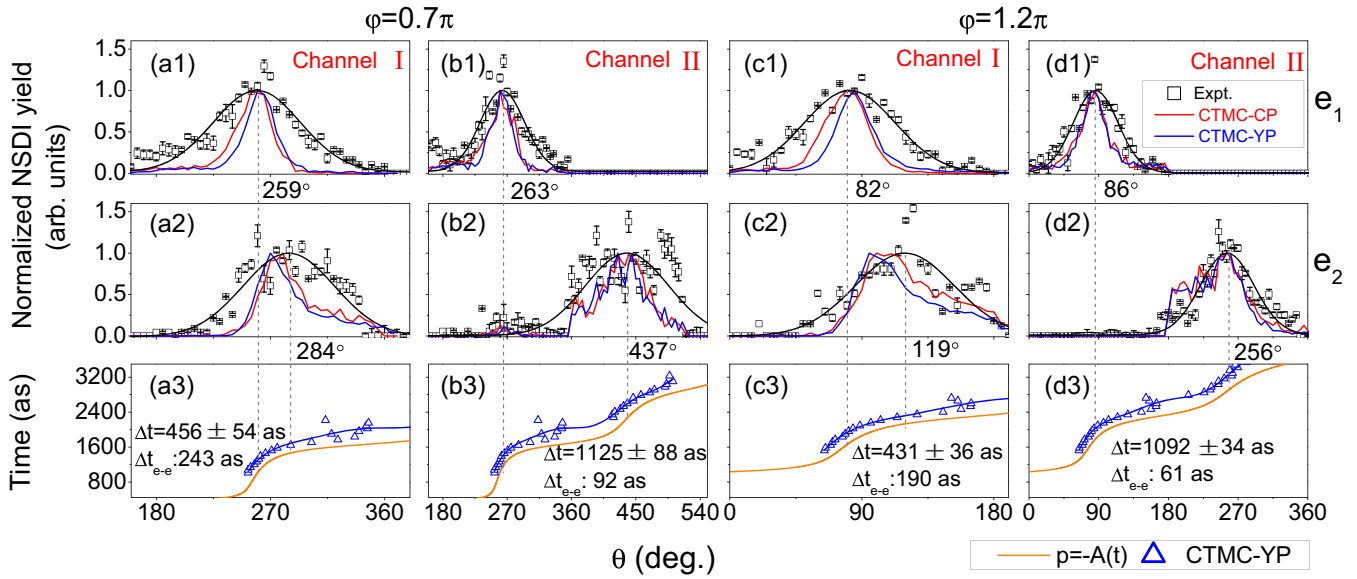

FIG. 3. (a1)–(d2) The measured angular distributions of the distinguished first and second ionized electrons for $\varphi = 0.7\pi$ and $\varphi = 1.2\pi$, respectively. The fitting curves with Gaussian function are depicted by the black lines. The error bars represent the standard deviations of multiple measurements. The red and blue lines correspond to the CTMC calculations with Coulomb potential (CP) and Yukawa potential (YP), respectively. (a3)–(d3) The time-angle relation obtained from $\mathbf{p} = -\mathbf{A}(t)$ (orange line) and the one derived from CTMC-YP model calculation (blue triangle), which is fitted with a polynomial function (blue line). The emission time difference, Δt, is determined by utilizing the time-angle relation derived from $\mathbf{p} = -\mathbf{A}(t)$ in the context of attoclock scheme. The uncertainties result from curve-fitting procedures. Additionally, $\Delta t_{e\text{-}e}$ denotes the emission time difference caused by the final-state e-e repulsion derived from the CTMC simulations including CP and YP.

with a short-range Yukawa potential $V_{ee} = e^{-\lambda r_b}/r_b$ once one electron is ionized from the DEC, where $r_b = \sqrt{(r_1 - r_2)^2 + b^2}$, $\lambda = 5.0$, and $b = 0.2$ [47]. The resulting angular distributions are shown in Figs. 3(a1)–3(d2) with blue lines. By mapping the peaks of these angular distributions to emission times and comparing with the results from the CTMC-CP calculations, the influence of final-state e-e repulsion can be quantitatively extracted. As illustrated in Figs. 3(a3)–3(d3), the emission time difference resulting from the final-state e-e repulsion (referred to as Δt_{e-e}) exerts a significant impact on Channel I, while exhibiting a relatively small influence on Channel II. Furthermore, we present the time-angle relation of the electron obtained from the CTMC-YP model calculation [blue triangles and lines in Figs. 3(a3)–3(d3)] and analyze the influence of the ionic Coulomb potential when converting angle into absolute emission time. It can be seen that the ionic Coulomb potential induces a similar shift in the absolute emission time of the first and second ionized electrons derived from the relation $\mathbf{p} = -\mathbf{A}(t)$ [see blue and orange lines], thereby allowing them to mutually cancel each other out.

Finally, we investigate the CEP dependence of the emission time difference of the two electrons in Channel I and Channel II. As depicted in Fig. 4(a), the emission time differences are found to be slightly changed at different CEPs for each channel. To understand the insensitivity of the obtained emission time difference to CEP, in Figs. 4(b) and 4(c), we show the energy distributions of the tunneling and bound electron trajectories at $0.05T$ before and after the recollision time t_r for two different CEPs. Figure 4(b) clearly shows that the energy distributions of the tunneling electrons before recollision are consistent and prominently concentrated around 0.5 a.u. for these CEPs. This leads to consistent energy distributions of the doubly excited states created during the recollision process, as depicted in Fig. 4(c). As a result, the two electrons will be emitted from these doubly excited states with similar emission time differences and insensitive to the CEP. Additionally, we present the mean emission time differences [indicated by dashed lines in Fig. 4(a)] for Channels I and II as 436 ± 13 as and 1113 ± 38 as, respectively. After accounting for the impact of the final-state e-e repulsion, the emission time differences are determined to be 234 ± 22 as and 1043 ± 73 as.

In conclusion, we propose a novel attoclock scheme utilizing a PG few-cycle laser pulse and demonstrate its application in timing the correlated-electron emission from a DEC generated in NSDI of argon under strong laser fields. The measured CEADs reveal distinct channels for double ionization and exhibit an angular difference between the two electrons. Our CTMC model calculations reproduce the experimental measurements well. By analyzing the angular distributions, we extract the emission time difference between the two electrons and quantitatively evaluate the influence of final-state e-e repulsion.

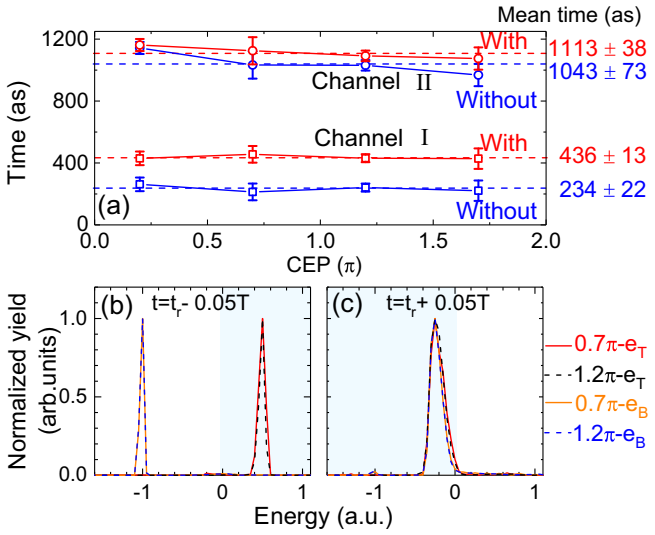

FIG. 4. (a) The measured emission time differences extracted for Channel I and Channel II under different CEPs with and without including the final-state e-e repulsion, respectively. The dashed line denotes the mean value. (b),(c) The energy distributions of the tunneling (e_T) and bound (e_B) electron trajectories at $0.05T$ before and after the recollision time t_r in CTMC-CP simulations for $\varphi = 0.7\pi$ and $\varphi = 1.2\pi$.

It is found that the most likely correlated emission time differences are 234 ± 22 as and 1043 ± 73 as for the two experimentally identified channels, respectively, and moreover, the time differences are insensitive to CEP of the PG pulse. The proposed PG attoclock scheme, as demonstrated in this work, provides a robust tool for tracing the correlated-electron emission in strong field atomic ionization, and could be extended to other more complex systems, such as molecules [30] or nanometric solids [54].

The authors acknowledge Lu Wang for helpful discussions. This letter is supported by the National Key Research and Development Program of China (No. 2019YFA0307700), the National Natural Science Foundation of China (No. 12121004, No. 12174401, No. 12004391, No. 12274420, and No. 12374240), Youth Innovation Promotion Association CAS (No. 2021328), CAS Project for Young Scientists in Basic Research (No. YSBR-091 and No. YSBR-055), and the Science and Technology Department of Hubei Province (No. 2021CFA078).

Appendix: 3D CTMC model calculation.—In this Appendix, we provide detailed information about the 3D CTMC model calculation, which has been successfully employed to understand the underlying physics behind the NSDI of Ar atom [47,48]. In the CTMC model, an outermost electron is assumed to be released into the continuum by quantum tunneling through the field-suppressed atomic potential. Subsequently, the propagation of this tunnel-ionized electron and a bound electron in the combined laser electric field and Coulomb field are described by the coupled classical Newton equations of motion,

$$\frac{d^2\mathbf{r_i}}{dt^2} = -\mathbf{E}(t) - \nabla_{\mathbf{r_i}}\left(V_{ne}^i + V_{ee}\right), \tag{A1}$$

where $i = 1, 2$ denote the two electrons, $\mathbf{E}(t)$ represents the PG electric field, $V_{ne}^i = -(2/|r_i|)$ is the Coulomb interaction between the nucleus and electron, and $V_{ee} = (1/|r_1 - r_2|)$ is the Coulomb repulsion between the two electrons.

In order to solve Eq. (A1), the initial conditions for the two electrons, i.e., the initial positions and velocities, have to be set up. For the tunnel-ionized electron, the tunneling exit $z_0 = -\frac{1}{2}\eta_0$ in a linearly polarized field can be obtained by solving the Schrödinger equation for an electron in a uniform field E [48,55]. In a PG pulse, the initial condition is obtained in the rotated coordinate the same as in the linearly polarized field and then projected to the original coordinate. At each tunneling moment t_0, the z axis is rotated to the direction of the instantaneous polarization. Thus, in the rotated coordinate, the initial positions x_0' and y_0' are set to 0, and $z_0' = -\frac{1}{2}\eta_0$ is introduced in the direction of the instantaneous polarization. As such, the initial positions in the original coordinate are $x_0 = z_0' \sin[\arctan(E_x/E_z)]$, $y_0 = 0$, and $z_0 = z_0' \cos[\arctan(E_x/E_z)]$. For the velocity in the rotated coordinate, the longitudinal velocity is assumed to be zero, while a nonzero initial velocity v_{per} is introduced in the perpendicular direction of the laser polarization. The corresponding initial velocities in the rotated coordinate are $v_{x0}' = v_{\mathrm{per}}\cos(\theta)$, $v_{y0}' = v_{\mathrm{per}}\sin(\theta)$, and $v_{z0}' = 0$. Thus, the initial velocity is obtained by projecting the rotated coordinate into the original coordinate: $v_{x0} = v_{x0}'\cos[\arctan(E_x/E_z)]$, $v_{y0} = v_{y0}'$, and $v_{z0} = -v_{x0}'\sin[\arctan(E_x/E_z)]$. The weight of each trajectory is evaluated as $w(t_0, v_{\mathrm{per}}) = w(0)w(1)$ [48,50], where

$$w(0) = \frac{4(2I_p)^2}{|E|}\exp\left[-2(2I_p)^{\frac{3}{2}}/3|E|\right] \tag{A2}$$

and

$$w(1) = \frac{v_{\mathrm{per}}(2I_p)^{\frac{1}{2}}}{|E|\pi}\exp\left[-v_{\mathrm{per}}^2(2I_p)^{\frac{1}{2}}/|E|\right]. \tag{A3}$$

Here, I_p is the ionization potential of Ar atom. For the bounded electron, the initial conditions are determined by assuming that it occupies the ground state of the singly charged argon ion Ar^+ and its initial distribution follows a microcanonical distribution.

The parameters in our calculations are given as follows: the ionization potential is $I_p = 0.58$ a.u., the peak intensity

of the two circularly polarized few-cycle pulses is about 3.35×10^{13} W/cm^2, corresponding to 8.5×10^{13} W/cm^2 for the combined laser field. 8×10^8 initial points are randomly distributed in the parameter space $-2\pi < \omega t_0 < 2\pi$, $0 < v_{\mathrm{per}} < 1$ a.u., and $0 < \theta < 2\pi$, so that the weight of the chosen trajectory is large enough. The evolution of this two-electron system is traced until the termination of the laser field using the classical Newton equation and a double ionization event is identified when the energies (a sum of kinetic plus potential energies) of both electrons are greater than zero. This results in more than 5×10^4 NSDI events in our statistics.

*These authors contributed equally to this letter.
†Corresponding author: xjliu@wipm.ac.cn

[1] J. Itatani, F. Quéré, G. L. Yudin, M. Yu. Ivanov, F. Krausz, and P. B. Corkum, Phys. Rev. Lett. **88**, 173903 (2002).
[2] A. L. Cavalieri, N. Müller, T. Uphues, V. S. Yakovlev, A. Baltuška, B. Horvath, B. Schmidt, L. Blümel, R. Holzwarth, S. Hendel, M. Drescher, U. Kleineberg, P. M. Echenique, R. Kienberger, F. Krausz, and U. Heinzmann, Nature (London) **449**, 1029 (2007).
[3] M. Schultze *et al.*, Science **328**, 1658 (2010).
[4] M. Ossiander, F. Siegrist, V. Shirvanyan, R. Pazourek, A. Sommer, T. Latka, A. Guggenmos, S. Nagele, J. Feist, J. Burgdörfer, R. Kienberger, and M. Schultze, Nat. Phys. **13**, 280 (2017).
[5] E. Goulielmakis, Z. H. Loh, A. Wirth, R. Santra, N. Rohringer, V. S. Yakovlev, S. Zherebtsov, T. Pfeifer, A. M. Azzeer, M. F. Kling, S. R. Leone, and F. Krausz, Nature (London) **466**, 739 (2010).
[6] A. Wirth, M. T. Hassan, I. Grguraš, J. Gagnon, A. Moulet, T. T. Luu, S. Pabst, R. Santra, Z. A. Alahmed, A. M. Azzeer, V. S. Yakovlev, V. Pervak, F. Krausz, and E. Goulielmakis, Science **334**, 195 (2011).
[7] P. Eckle, M. Smolarski, P. Schlup, J. Biegert, A. Staudte, M. Schöffler, H. G. Muller, R. Dörner, and U. Keller, Nat. Phys. **4**, 565 (2008).
[8] P. Eckle, A. N. Pfeiffer, C. Cirelli, A. Staudte, R. Dörner, H. G. Muller, M. Büttiker, and U. Keller, Science **322**, 1525 (2008).
[9] A. N. Pfeiffer, C. Cirelli, M. Smolarski, D. Dimitrovski, M. Abu-samha, L. B. Madsen, and U. Keller, Nat. Phys. **8**, 76 (2012).
[10] R. Ramos, D. Spierings, I. Racicot, and A. M. Steinberg, Nature (London) **583**, 529 (2020).
[11] A. S. Landsman, M. Weger, J. Maurer, R. Boge, A. Ludwig, S. Heuser, C. Cirelli, L. Gallmann, and U. Keller, Optica **1**, 343 (2014).
[12] N. Camus, E. Yakaboylu, L. Fechner, M. Klaiber, M. Laux, Y. Mi, K. Z. Hatsagortsyan, T. Pfeifer, C. H. Keitel, and R. Moshammer, Phys. Rev. Lett. **119**, 023201 (2017).
[13] T. Zimmermann, S. Mishra, B. R. Doran, D. F. Gordon, and A. S. Landsman, Phys. Rev. Lett. **116**, 233603 (2016).
[14] M. Han, P. P. Ge, Y. Q. Fang, X. Y. Yu, Z. N. Guo, X. Y. Ma, Y. K. Deng, Q. H. Gong, and Y. Q. Liu, Phys. Rev. Lett. **123**, 073201 (2019).
[15] U. S. Sainadh, H. Xu, X. S. Wang, A. Atia-Tul-Noor, W. C. Wallace, N. Douguet, A. Bray, I. Ivanov, K. Bartschat, A. Kheifets, R. T. Sang, and I. V. Litvinyuk, Nature (London) **568**, 75 (2019).
[16] L. Torlina, F. Morales, J. Kaushal, I. Ivanov, A. Kheifets, A. Zielinski, A. Scrinzi, H. G. Muller, S. Sukiasyan, M. Ivanov, and O. Smirnova, Nat. Phys. **11**, 503 (2015).
[17] W. Quan, V. V. Serov, M. Z. Wei, M. Zhao, Y. Zhou, Y. L. Wang, X. Y. Lai, A. S. Kheifets, and X. J. Liu, Phys. Rev. Lett. **123**, 223204 (2019).
[18] H. Ni, U. Saalmann, and J. M. Rost, Phys. Rev. Lett. **117**, 023002 (2016).
[19] N. Eicke and M. Lein, Phys. Rev. A **97**, 031402(R) (2018).
[20] J. H. Tong, X. W. Liu, W. H. Dong, W. Y. Jiang, M. Zhu, Y. D. Xu, Z. T. Zuo, P. F. Lu, X. C. Gong, X. H. Song, W. F. Yang, and J. Wu, Phys. Rev. Lett. **129**, 173201 (2022).
[21] V. Hanus, S. Kangaparambil, S. Larimian, M. Dorner-Kirchner, X. H. Xie, M. S. Schöffler, G. G. Paulus, A. Baltuška, A. Staudte, and M. Kitzler-Zeiler, Phys. Rev. Lett. **124**, 103201 (2020).
[22] A. N. Pfeiffer, C. Cirelli, M. Smolarski, R. Dörner, and U. Keller, Nat. Phys. **7**, 428 (2011).
[23] Y. Zhou, C. Huang, Q. Liao, and P. Lu, Phys. Rev. Lett. **109**, 053004 (2012).
[24] X. Wang, J. Tian, and J. H. Eberly, Phys. Rev. Lett. **110**, 073001 (2013).
[25] A. Fleischer, H. J. Wörner, L. Arissian, L. R. Liu, M. Meckel, A. Rippert, R. Dörner, D. M. Villeneuve, P. B. Corkum, and A. Staudte, Phys. Rev. Lett. **107**, 113003 (2011).
[26] C. M. Maharjan, A. S. Alnaser, X. M. Tong, B. Ulrich, P. Ranitovic, S. Ghimire, Z. Chang, I. V. Litvinyuk, and C. L. Cocke, Phys. Rev. A **72**, 041403(R) (2005).
[27] M. S. Schöffler, X. H. Xie, P. Wustelt, M. Möller, S. Roither, D. Kartashov, A. M. Sayler, A. Baltuska, G. G. Paulus, and M. Kitzler, Phys. Rev. A **93**, 063421 (2016).
[28] B. Walker, B. Sheehy, L. F. DiMauro, P. Agostini, K. J. Schafer, and K. C. Kulander, Phys. Rev. Lett. **73**, 1227 (1994).
[29] A. Becker, R. Dörner, and R. Moshammer, J. Phys. B **38**, S753 (2005).
[30] W. Becker, X. J. Liu, P. J. Ho, and J. H. Eberly, Rev. Mod. Phys. **84**, 1011 (2012).
[31] C. Faria and X. Liu, J. Mod. Opt. **58**, 1076 (2011).
[32] P. Dietrich, N. H. Burnett, M. Ivanov, and P. B. Corkum, Phys. Rev. A **50**, R3585 (1994).
[33] Z. H. Chang, Phys. Rev. A **70**, 043802 (2004).
[34] B. Shan, S. Ghimire, and Z. H. Chang, J. Mod. Opt. **52**, 277 (2005).
[35] I. J. Sola, E. Mével, L. Elouga, E. Constant, V. Strelkov, L. Poletto, P. Villoresi, E. Benedetti, J. P. Caumes, S. Stagira, C. Vozzi, G. Sansone, and M. Nisoli, Nat. Phys. **2**, 319 (2006).
[36] G. Sansone, E. Benedetti, F. Calegari, C. Vozzi, L. Avaldi, R. Flammini, L. Poletto, P. Villoresi, C. Altucci, R. Velotta, S. Stagira, S. De Silvestri, and M. Nisoli, Science **314**, 443 (2006).
[37] Y. L. Wang, S. G. Yu, X. Y. Lai, H. P. Kang, S. P. Xu, R. P. Sun, W. Quan, and X. J. Liu, Phys. Rev. A **98**, 043422 (2018).

[38] R. P. Sun, Y. L. Wang, Y. Zhou, S. G. Yu, S. P. Xu, X. Y. Lai, W. Quan, and X. J. Liu, Phys. Rev. A **105**, L021103 (2022).
[39] D. I. Bondar, W. K. Liu, and M. Y. Ivanov, Phys. Rev. A **79**, 023417 (2009).
[40] N. Camus, B. Fischer, M. Kremer, V. Sharma, A. Rudenko, B. Bergues, M. Kübel, N. G. Johnson, M. F. Kling, T. Pfeifer, J. Ullrich, and R. Moshammer, Phys. Rev. Lett. **108**, 073003 (2012).
[41] C. Huang, W. L. Guo, Y. M. Zhou, and Z. M. Wu, Phys. Rev. A **93**, 013416 (2016).
[42] R. Gopal, K. Simeonidis, R. Moshammer, T. Ergler, M. Dürr, M. Kurka, K. U. Kühnel, S. Tschuch, C. D. Schröter, D. Bauer, J. Ullrich, A. Rudenko, O. Herrwerth, T. Uphues, M. Schultze, E. Goulielmakis, M. Uiberacker, M. Lezius, and M. F. Kling, Phys. Rev. Lett. **103**, 053001 (2009).
[43] W. Quan, M. H. Yuan, S. G. Yu, S. P. Xu, Y. J. Chen, Y. L. Wang, R. P. Sun, Z. L. Xiao, C. Gong, L. Q. Hua, X. Y. Lai, X. J. Liu, and J. Chen, Opt. Express **24**, 23248 (2016).
[44] R. Dörner, V. Mergel, O. Jagutzki, L. Spielberger, J. Ullrich, R. Moshammer, and H. Schmidt-Böcking, Phys. Rep. **330**, 95 (2000).
[45] J. Ullrich, R. Moshammer, A. Dorn, R. Dörner, L. Ph. H. Schmidt, and H. Schmidt-Böcking, Rep. Prog. Phys. **66**, 1463 (2003).
[46] R. P. Sun, X. Y. Lai, S. G. Yu, Y. L. Wang, S. P. Xu, W. Quan, and X. J. Liu, Phys. Rev. Lett. **122**, 193202 (2019).
[47] D. F. Ye, X. Liu, and J. Liu, Phys. Rev. Lett. **101**, 233003 (2008).
[48] Y. L. Wang, S. P. Xu, Y. J. Chen, H. P. Kang, X. Y. Lai, W. Quan, X. J. Liu, X. L. Hao, W. D. Li, S. L. Hu, J. Chen, W. Becker, W. Chu, J. P. Yao, B. Zeng, Y. Cheng, and Z. Z. Xu, Phys. Rev. A **95**, 063415 (2017).
[49] Note that the momentum of the undetected electron is obtained by employing the momentum conservation in the double ionization process. Consequently, due to the thermal momentum of the argon atom beam in a cold target recoil ion momentum spectrometer, a broad electron momentum distribution along the x direction leads to a wider angular distribution in the data than in CTMC simulation.
[50] N. B. Delone and V. P. Krainov, J. Opt. Soc. Am. B **8**, 1207 (1991).
[51] H. Kang, K. Henrichs, M. Kunitski, Y. Wang, X. Hao, K. Fehre, A. Czasch, S. Eckart, L. Ph. H. Schmidt, M. Schöffler, T. Jahnke, X. Liu, and R. Dörner, Phys. Rev. Lett. **120**, 223204 (2018).
[52] F. Faisal, J. Phys. B **6**, L89 (1973).
[53] H. Reiss, Phys. Rev. A **22**, 1786 (1980).
[54] S. Meier, J. Heimerl, and P. Hommelhoff, Nat. Phys. **19**, 1402 (2023).
[55] B. Hu, J. Liu, and S. G. Chen, Phys. Lett. A **236**, 533 (1997).